Supporting Information

Beilstein et al. 10.1073/pnas.0909766107

SI Materials and Methods

Evaluation of Potential Fossil Calibrations. We searched the paleobotanical literature and identified 32 fossils assigned to Brassicales (Table S1). Only six (*Akania americana, Akania patagonica, Akania* sp., *Capparidoxylon holleisii*, *Dressiantha bicarpellata*, *Thlaspi primaevum*) could be placed confidently in Brassicales. A fossil was considered acceptable for use as an age constraint only if its record included a clear citation with photographic evidence or accurate reproduction, fossil collection number, and morphological characters that support the proposed placement.

Ultrametric Tree and Divergence Date Estimation. To calculate divergence dates for Brassicales, we first inferred trees from plastid *ndh*F and the nuclear locus phytochrome A (*PHYA*) data separately and then from combined *ndh*F and *PHYA* data (Table S2). The *ndh*F alignment comprised 2,067 nucleotide positions representing 170 species in the order Brassicales plus *Gossypium gossypioides* (Malvales). The *PHYA* alignment comprised 1,824 nucleotide positions representing 149 accessions from 139 species in the order Brassicales. The combined alignment comprised 3,798 nucleotide positions representing 177 species of Brassicales plus *G. gossypioides*. The combined matrix included species missing data for one of the two genes (i.e., seven species lack *ndh*F data; 38 species lack *PHYA* data). However, for all major lineages of Brassicales, there is at least one taxon in the matrix represented by both *ndh*F and *PHYA* data.

We inferred trees with branch lengths from all three datasets using the general time reversible (GTR) model and Γ distributed rate heterogeneity in RAxML v. 7.2.3 (1). In analyses of the combined dataset, we allowed each gene to evolve independently. Trees resulting from these analyses were used to calculate ultrametric trees with divergence dates using the penalized likelihood (PL) approach in r8s v. 1.71 (2). PL employs a smoothing parameter to correlate substitution rates across the tree (3), thereby accounting for variation in substitution rates among branches. We performed cross-validation (2) over a range of smoothing parameters to determine that the best smoothing value for the *ndh*F tree is 32 ($10^{1.5}$), for the *PHYA* tree is 25 ($10^{1.4}$), and for the combined tree is 32 ($10^{1.5}$). For all analyses in r8s, *Dressiantha bicarpellata* was designated a fixed age constraint, and all other fossil dates were used as minimum age constraints.

Because the position of *D. bicarpellata* is uncertain, and because we used it as a fixed age constraint in all r8s analyses, we explored the impact on age estimates from r8s of placing this fossil at different nodes in the tree. We determined the most likely positions by analyzing a matrix of combined *ndh*F and morphology data developed from the published morphological dataset for extant Brassicales (4) and scoring characters for *D. bicarpellata* as described in Gandolfo et al. (5). We analyzed the combined data using a mixed model in MrBayes 3.2 (6) and used Mesquite 2.71 (7) to sort the resulting 19,000 post–burn-in trees. The most frequently visited topology from this analysis placed *D. bicarpellata* sister to *Moringa oleifera*. Two other frequently visited topologies placed *D. bicarpellata* sister to *Carica papaya* or *Batis maritima*. Based on these results, we analyzed the *ndh*F, *PHYA*, and combined trees, placing the *D. bicarpellata* constraint at different nodes in the inferred trees (Table S3). We found that the position of the *D. bicarpellata* fixed age constraint has only a moderate impact on the ages of more-derived nodes in the tree. For example, in the *ndh*F analyses, the optimal age of the *Arabidopsis* crown group is 19 Mya when *D. bicarpellata* is placed at the deepest node of the tree and 20.8 Mya for the most-derived node calibration (Table S3).

All other fossils were used as minimum age constraints in r8s. We calibrated two different nodes with the *Akania* fossils; the *Akania americana*/*A. patagonica* fossils are from a more recent deposit than *Akania* sp. (Table S1), and thus we used the younger date for these fossils to constrain the divergence of *Akania bidwillii* and *Bretschneidera sinensis*. *Akania* sp. was used to constrain the node defined by *A. bidwilli* and *Tropaeolum majus*, which is deeper in the tree than the split constrained by *A. americana*/*A. patagonica*. This strategy allowed us to use all *Akania* fossils as calibrations in the *ndh*F and combined analyses. We lacked *PHYA* data for *B. sinensis*, precluding the use of *A. americana*/*A. patagonica* as a calibration in *PHYA* analyses. Morphological analysis of *Capparidoxylon holleisii* using Inside Wood (8) indicated affinities between *C. holleisii* and extant *Capparis*, and thus this fossil was placed at the coalescence of *Capparis hastata* with other Capparaceae. However, exploration of the effect of this calibration by its removal and subsequent reanalysis of node ages indicated that it had no effect on the dates of other nodes in the tree, and thus it was excluded from subsequent analyses. We placed the fossil *Thlaspi primaevum* at the coalescence of *Thlaspi arvense* and *Alliaria petiolata* based on the presence of striated seeds (unique to these two genera among extant Brassicaceae; Fig. S1) and on likelihood ancestral character state reconstruction of fruit morphology using the Mk1 model of evolution (9) in Mesquite (7) with character state transition rates estimated from the data. Ancestral traits were inferred on a likelihood tree with branch lengths generated from an analysis of combined *ndhF* and *PHYA* data for Brassicaceae using RAxML (1). The ancestral character state reconstruction indicates that within this clade angustiseptate fruits evolved along the branch leading to *T. arvense* (Fig. S1). We also explored the effect of *T. primaevum* as a calibration point in r8s by excluding it from the r8s analyses (Table S4).

We inferred divergence dates on the *ndh*F tree using five fossil calibrations (*A. americana*/*A. patagonica*, 47.5 Mya; *Akania* sp., 61.7 Mya; *Dressiantha bicarpellata*, 89.3 Mya; and *T. primaevum*, 29.0 Mya; Table S1). For all *ndh*F analyses in r8s, we rooted with *G. gossypioides*, and thus it was pruned from the tree before divergence dates were estimated.

We explored alternative tree-rooting strategies to infer divergence dates for the *PHYA* tree in r8s. We found only a partial *PHYA* fragment for *G. gossypioides* from an expressed sequence tag, and inclusion of this sequence in the *PHYA* phylogenetic analysis produced trees with ingroup topologies inconsistent with trees inferred from other data. Instead, we rooted our Brassicales *PHYA* tree with *Akania bidwillii* + *Tropaeolum majus* [the first diverging lineage resolved in analyses by Hall et al. (10) and Rodman et al. (4, 11)], which yielded an ingroup topology consistent with other trees. However, it precluded the use of the *Akania* fossil constraint, because the root node was pruned before inferring dates. Thus, our *PHYA* r8s analysis used two age constraints: *D. bicarpellata* as a fixed age constraint and *T. primaevum* as a minimum age constraint.

Our analysis of the combined *ndh*F/*PHYA* tree using r8s was similar to the *ndh*F single-gene analysis. The tree was rooted with *G. gossypioides*, which was pruned in r8s before dates were inferred. The four fossil calibration points used in the *ndh*F analysis were used to calibrate nodes in the combined analysis with *D. bicarpellata* as a fixed age constraint and all others as minimum age constraints.

We also used BEAST v. 1.5.3 (12, 13) to calculate divergence dates from each gene individually and from the combined *ndh*F and *PHYA* data (Figs. S2–S4). We allowed BEAST to infer the tree, branch lengths, and dates in analyses of the *ndh*F and combined data. Because of sparser taxon sampling and the presence of a long branch to *Gyrostemon tepperi*, attempts to infer trees and dates simultaneously from the *PHYA* data using BEAST resulted in topologies and dates inconsistent with our RAxML, r8s, and BEAST analyses of the *ndh*F and combined data. Thus, we fixed the *PHYA* topology to that which was used to infer dates using r8s but allowed BEAST to alter all other aspects of the model of evolution while inferring dates.

All our analyses in BEAST accounted for rate variation by using an uncorrelated relaxed clock drawn from a lognormal distribution that allows different rates to be optimized independently on each branch of the tree (13). In addition, the likelihood of speciation was described by the Yule process (14), and branch rates were determined under a GTR + Γ model of nucleotide evolution with four rate categories (13). In the analysis of combined data we unlinked the substitution model and clock model, allowing each data partition to evolve independently across the same tree. We used a uniform distribution for all four fossil calibrations with the lower hard bound of the distribution set to the age of the fossil (i.e., *A. americana*/*A. patagonica*, 47 Mya; *Akania* sp., 61 Mya; *D. bicarpellata*, 89.3 Mya; *T. primaevum*, 29 Mya). Upper hard bounds were set to the age of the oldest eudicot pollen (125 Mya) (15) for *D. bicarpellata* and *A.* sp. and were defined by the age of other fossils in the analysis for *A. americana*/*A. patagonica* (no older than *A.* sp., 61 Mya) and *T. primaevum* (no older than *D. bicarpellata*, 89.3 Mya). We also used a prior on the age of the root node which was set with a hard upper bound defined by the age of the oldest fossil eudicot pollen and the lower bound set to be no younger than the age of *D. bicarpellata* (89.3 Mya). The *A. americana*/*A. patagonica* fossil calibration was not used in the *PHYA* analysis because we lacked *PHYA* data from *Bretschneidera sinensis*.

We allowed BEAST to run for 3×10^7 generations saving data every 1,000 generations for *ndh*F, *PHYA*, and combined analyses. Convergence statistics for each run were analyzed in Tracer v. 1.4.1 (16), resulting in 27,000 post–burn-in generations. We tuned the performance of the BEAST analyses from the initial runs using performance-tuning suggestions generated in the initial analyses. Then a second set of BEAST analyses with tuned operators was performed. The *ndh*F and *PHYA* analyses were run for 3×10^7 generations, and the combined analysis was run for 6×10^7 generations. Convergence statistics for each run were analyzed in Tracer. We used TreeAnnotator v. 1.5.3 (13) to produce a maximum clade credibility tree from the post–burn-in trees and to determine the 95% probability density of ages for all nodes in the tree (Figs. S2–S4).

Species Diversification Rate. We used LASER v. 2.2 (17) in R (18) to test for significant shifts in net diversification rate over the history of Brassicales. LASER applies a likelihood framework based on a birth–death model to identify whether a constant rate or two-rate model better fits the data (a chronogram for which the species diversity of the terminal taxa is known). The most likely shift point in the chronogram is identified by splitting the tree at each branch to determine whether the data are better described by a constant rate model (a single diversification rate across the tree) or a two-rate model (one rate before the split and a second rate after). The node giving the maximum combined log-likelihood for the two partitions (i.e., before and after the rate shift) is the maximum likelihood estimate of the shift point on the tree. Inputs for the analysis include (*i*) a pruned chronogram and (*ii*) a table of species diversity for each lineage retained in the pruned chronogram.

For all three datasets, we pruned the Brassicales chronogram from BEAST (Figs. S2–S4) to a single representative from each family, except Brassicaceae where we retained *Aethionema* as an independent lineage to test whether a significant rate shift occurred after the divergence of *Aethionema* from all other Brassicaceae. Other lineages retained in the *ndh*F and combined analyses included *Forchhammeria* and *Tirania*; these lineages are not present in the *PHYA* tree. Branch lengths were maintained during the pruning process. Clade diversity for each group was determined from the Angiosperm Phylogeny Website (19). We calculated the likelihoods of our phylogenetic data under a model of constant diversification rate over time and under a two-rate model in which the diversification rate is permitted to change (Table S5). Because analyses of diversification rate can be sensitive to extinction, we determined whether our results were sensitive to differences in extinction fraction by reanalyzing the data under low ($a = 0$) and high ($a = 0.99$) extinction fractions (Table S5). The branch leading to the core Brassicales was the locus of the shift under both high and low extinction for the combined tree, high extinction for the *ndh*F tree, and low extinction for the *PHYA* tree. Analyses assuming a low extinction fraction across the *ndh*F tree or a high extinction fraction across the *PHYA* tree placed the locus of the rate shift one node deeper (toward the base) of the tree (Table S5). In all analyses, the two-rate model was significantly better than the constant rate model, regardless of extinction fraction (Table S5). Although the two-rate and rate-decrease models cannot be compared by likelihood ratio test, our results suggest that the two-rate model may fit the data better than the rate-decrease model (Table S5). Taken together, our results indicate a significant shift in species diversification rate either along the branch leading to core Brassicales or before the divergence of core Brassicales from its sister clade.

1. Stamatakis A (2006) RAxML-VI-HPC: Maximum likelihood-based phylogenetic analyses with thousands of taxa and mixed models. *Bioinformatics* 22:2688–2690.
2. Sanderson MJ (2003) r8s: Inferring absolute rates of molecular evolution and divergence times in the absence of a molecular clock. *Bioinformatics* 19:301–302.
3. Sanderson MJ (2002) Estimating absolute rates of molecular evolution and divergence times: A penalized likelihood approach. *Mol Biol Evol* 19:101–109.
4. Rodman JE, Karol KG, Price RA, Sytsma KJ (1996) Molecules, morphology, and Dahlgren's expanded Order Capparales. *Systematic Botany* 21:289–307.
5. Gandolfo MA, Nixon KC, Crepet WL (1998) A new fossil flower from the Turonian of New Jersey: *Dressiantha bicarpellata* gen. et sp. nov. (Capparales). *Am J Bot* 85:964–974.
6. Ronquist FR, Huelsenbeck JP (2003) MrBayes 3: Bayesian phylogenetic inference under mixed models. *Bioinformatics* 19:1572–1574.
7. Maddison WP, Maddison DR (2009) Mesquite: A modular system for evolutionary analysis Version 2.6. Available at http://mesquiteproject.org.
8. Wheeler EA (2004) Inside Wood. Available at: http://insidewood.lib.ncsu.edu/. Accessed June 18, 2009.
9. Lewis PO (2001) A likelihood approach to estimating phylogeny from discrete morphological character data. *Systematic Botany* 50:913–925.
10. Hall JC, Iltis HH, Sytsma KJ (2004) Molecular phylogenetics of core Brassicales, placement of orphan genera *Emblingia, Forchhammeria, Tirania*, and character evolution. *Systematic Botany* 29:654–669.
11. Rodman J, et al. (1993) Nucleotide sequences of the *rbc*L gene indicate monophyly of mustard oil plants. *Ann Mo Bot Gard* 80:686–699.
12. Drummond AJ, Ho SYW, Phillips MJ, Rambaut A (2006) Relaxed phylogenetics and dating with confidence. *PLoS Biol* 4:e88.
13. Drummond AJ, Rambaut A (2007) BEAST: Bayesian evolutionary analysis by sampling trees. *BMC Evol Biol* 7:214.
14. Yule GU (1924) A mathematical theory of evolution based on the conclusions of Dr. J.C. Willis. *Philos Trans R Soc Lond B Biol Sci* 213:21–87.
15. Brenner GJ (1996) Evidence of the earliest stage of angiosperm pollen evolution: A paleoequatorial section from Israel. *Flowering Plant Origin, Evolution and Phylogeny*, eds Taylor DW, Hickey LJ (Chapman and Hall, New York), pp 91–115.
16. Rambaut A, Drummond AJ (2003) *Tracer 1.4.* Available at http://tree.bio.ed.ac.uk/software/tracer. Accessed June 18, 2009.
17. Rabosky DL (2006) LASER: A maximum likelihood toolkit for detecting temporal shifts in diversification rates from molecular phylogenies. *Evol Bioinf Online* 247–250.
18. R Development Core Team (2008) *R: A Language and Environment for Statistical Computing* (R Foundation for Statistical Computing, Vienna).
19. Stevens PF (2001 onwards) Angiosperm Phylogeny Website. Version 9. (http://www.mobot.org/MOBOT/research/APweb/). Accessed June 18, 2009.

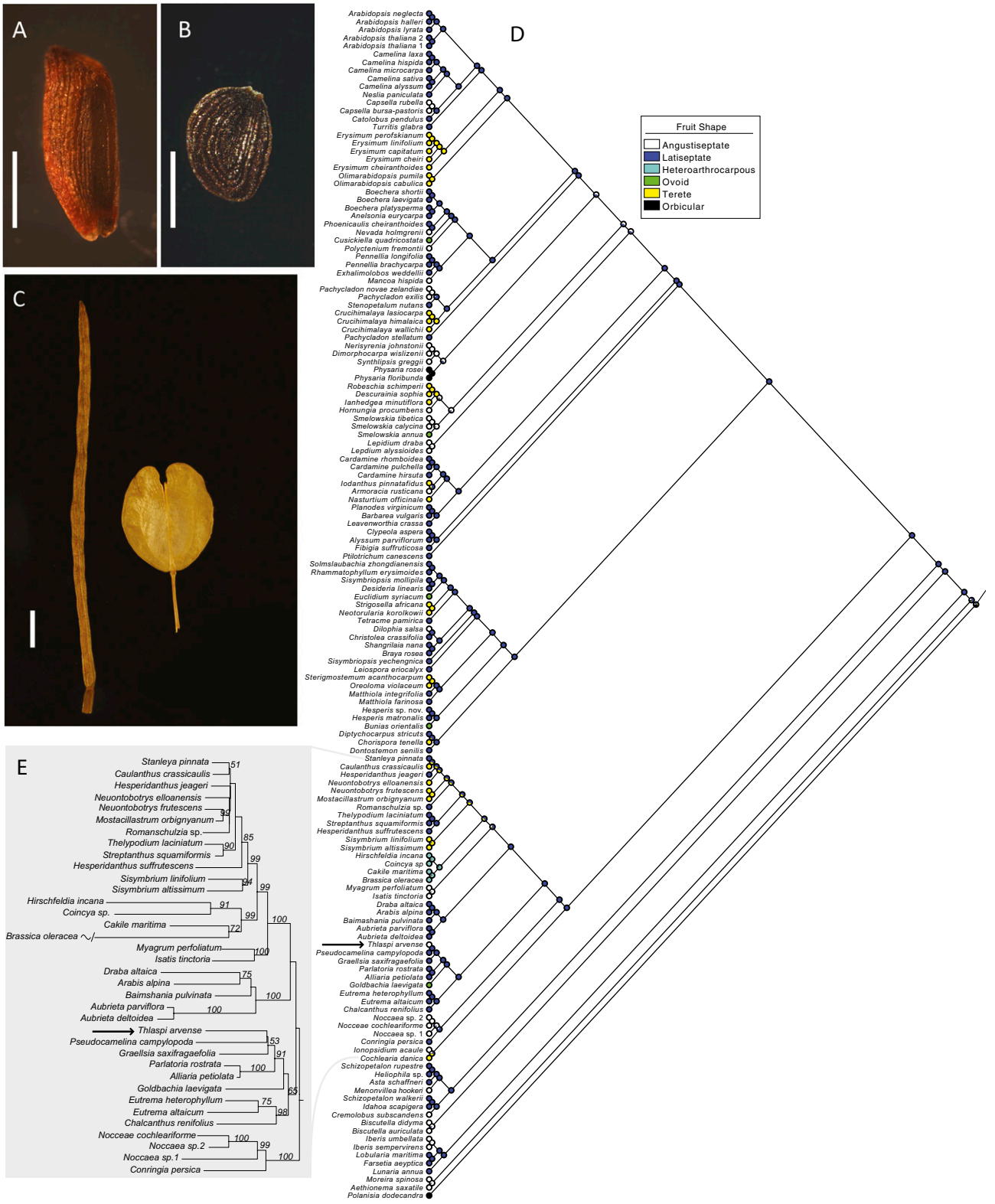

Fig. S1. Comparison of *Alliaria petiolata* and *Thlaspi arvense*, with likelihood character state reconstruction using the Mk1 (1) model in Mesquite (2). Seeds of (*A*) *A. petiolata* with longitudinal striations and (*B*) *T. arvense* with concentrically curved striations. (Scale bar, 1 mm.) (*C*) Latiseptate *A. petiolata* fruit (*Left*) and angustiseptate *T. arvense* fruit (*Right*). (Scale bar, 5 mm.) (*D*) Likelihood reconstruction for fruit type in Brassicaceae indicating that angustiseptate fruits evolved along the branch to *T. arvense* in the clade defined by *T. arvense* (arrow) and *A. petiolata*. (*E*) Likelihood branch-length tree showing bootstrap support from 100 replicates for the clade that includes *T. arvense* (arrow) and *A. petiolata*.

1. Lewis PO (2001) A likelihood approach to estimating phylogeny from discrete morphological character data. *Systematic Botany* 50:913–925.
2. Maddison WP, Maddison DR (2009) Mesquite: A modular system for evolutionary analysis. Version 2.6. http://mesquiteproject.org. Accessed June 18, 2009.

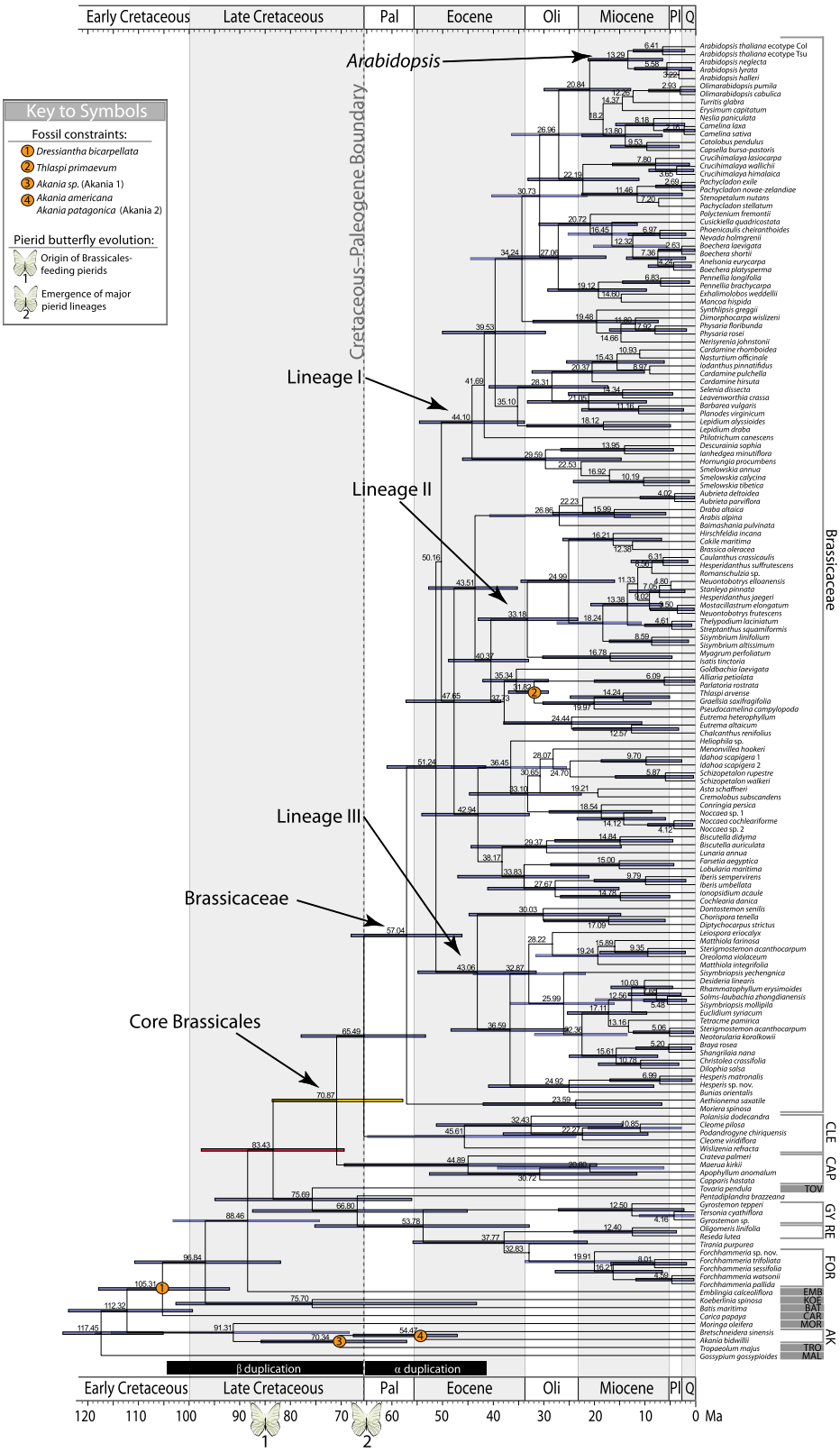

Fig. S2. Maximum clade credibility chronogram of *ndh*F from BEAST with 95% highest probability density (HPD) for node ages (blue bars along branches). The red HPD bar denotes the branch along which a significant shift in speciation rate occurred when extinction is low. The yellow HPD bar denotes the branch when extinction is high (Table S5). Numbers above nodes are means of the probability density distribution. Black bars indicate putative range of α and β whole-genome duplications. See figure for key to symbols. Abbreviated taxonomic groups are AK, Akaniaceae; BAT, Bataceae; CAP, Capparaceae; CAR, Caricaceae; CLE, Cleomaceae; GY, Gyrostemonaceae; KOE, Koeberlineaceae; MAL, Malvaceae; MOR, Moringaceae; RE, Resedaceae; Tro, Tropaeolaceae; and FOR, the genus *Forchhammeria*. Abbreviated geologic periods are Oli, Oligocene; Pal, Paleocene; Pl, Pliocene; and Q, Quaternary.

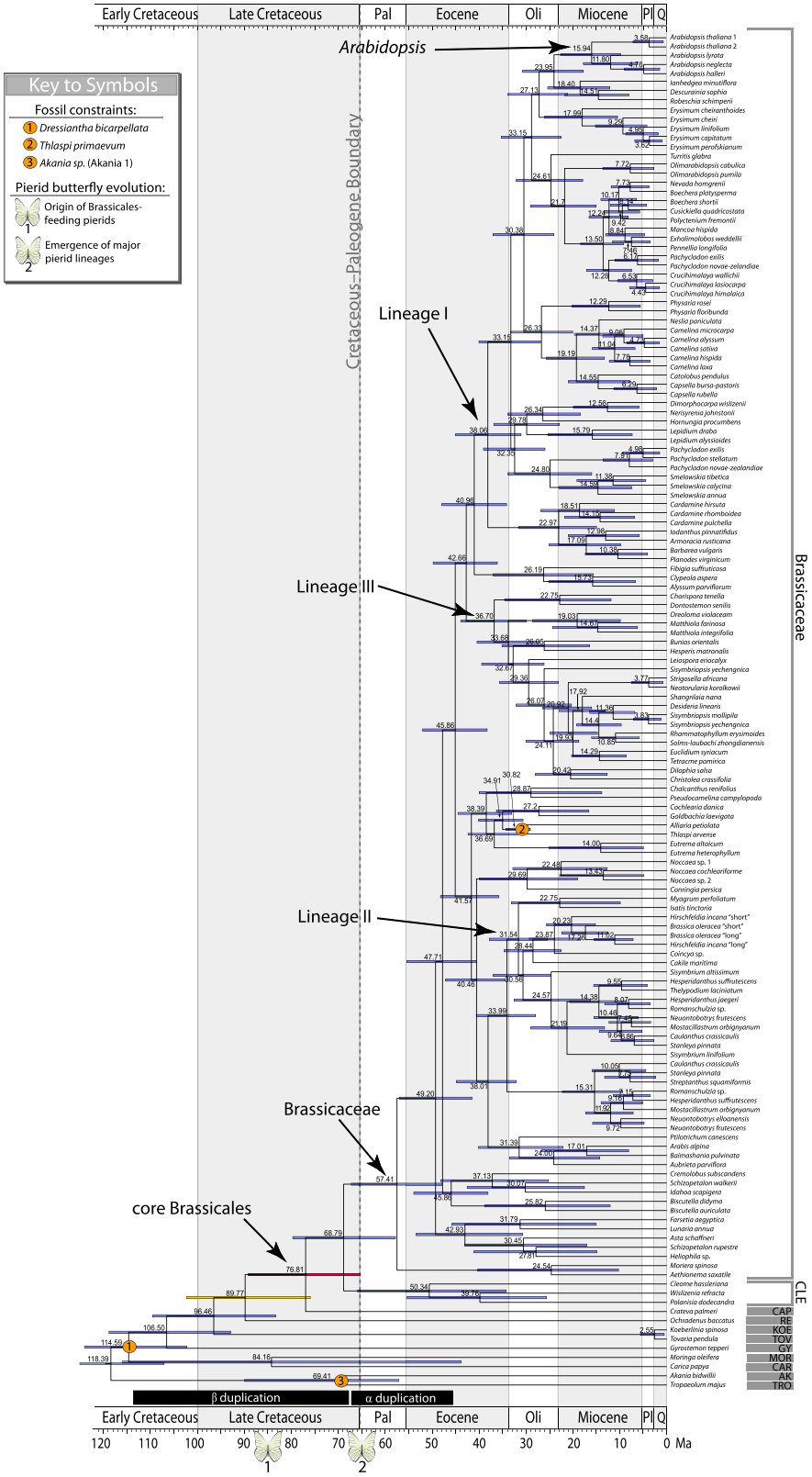

Fig. S3. Maximum clade credibility chronogram of *PHYA* from BEAST with 95% HPD for node ages (blue bars along branches). The red HPD bar denotes the branch along which a significant shift in speciation rate occurred when extinction is low. The yellow HPD bar denotes the branch when extinction is high (Table S5). Numbers above nodes are means of the probability density distribution. Black bars indicate putative range of α and β whole-genome duplications. See figure for key to symbols. Abbreviated taxonomic groups are AK, Akaniaceae; BAT, Bataceae; CAP, Capparaceae; CAR, Caricaceae; CLE, Cleomaceae; GY, Gyrostemonaceae; KOE, Koeberlineaceae; MOR, Moringaceae; RE, Resedaceae; TRO, Tropaeolaceae; and FOR, the genus *Forchhammeria*. Abbreviated geologic periods are Oli, Oligocene; Pal, Paleocene; Pl, Pliocene; and Q, Quaternary.

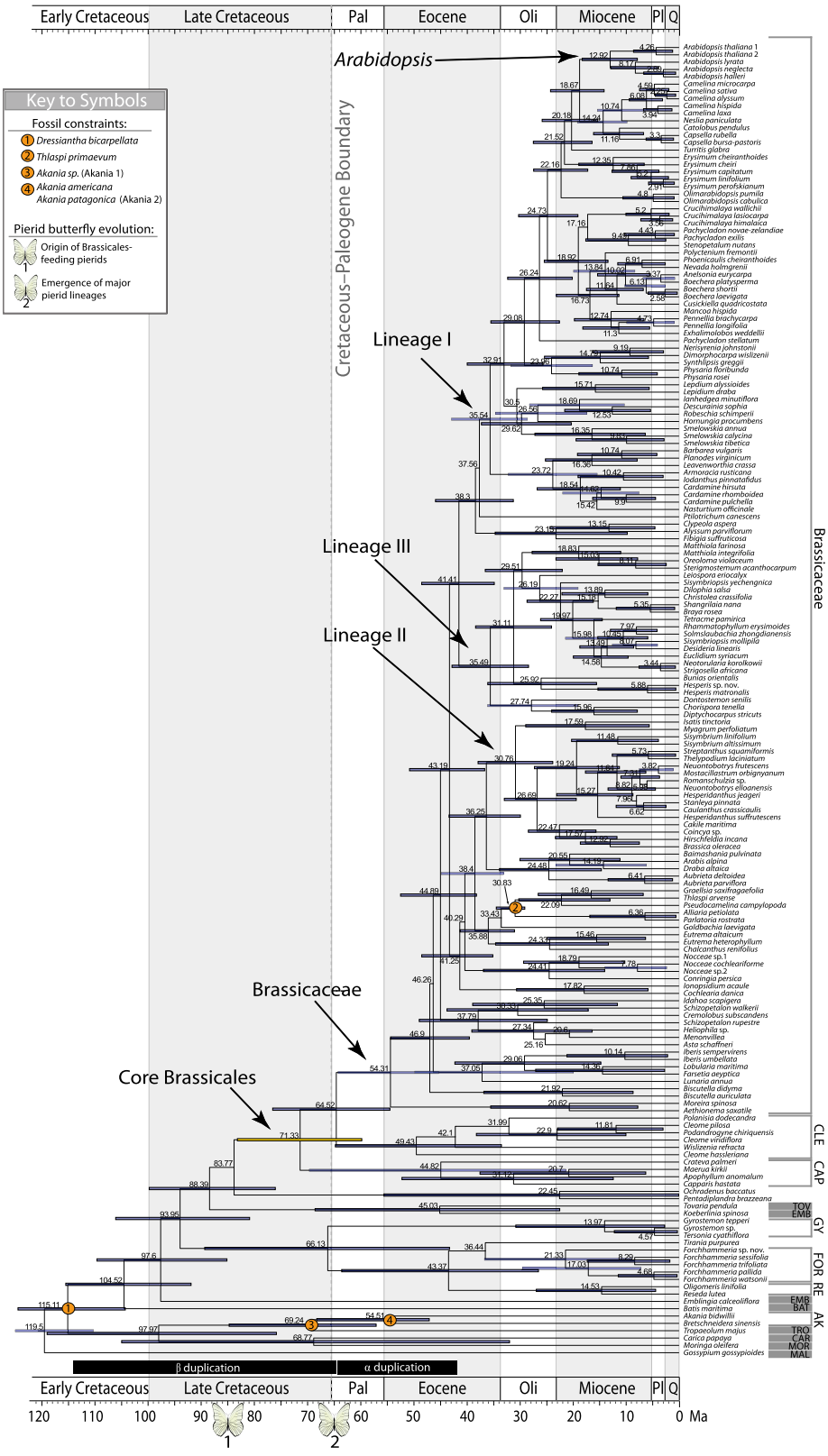

Fig. S4. Maximum clade credibility chronogram of *ndh*F/*PHYA* combined data from BEAST with 95% HPD for node ages (blue bars along branches). The yellow HPD bar denotes the branch along which a significant shift in speciation rate occurred (Table S5). Numbers above nodes are means of the probability density distribution. Black bars indicate putative range of α and β whole-genome duplications. See figure for key to symbols. Abbreviated taxonomic groups are AK, Akaniaceae; BAT, Bataceae; CAP, Capparaceae; CAR, Caricaceae; CLE, Cleomaceae; GY, Gyrostemonaceae; KOE, Koeberlineaceae; MAL, Malvaceae; MOR, Moringaceae; RE, Resedaceae; TRO, Tropaeolaceae; and FOR, the genus *Forchhammeria*. Abbreviated geologic periods are Oli, Oligocene; Pal, Paleocene; Pl, Pliocene; and Q, Quaternary.

Other Supporting Information Files

Table S1 (DOCX)
Table S2 (DOCX)
Table S3 (DOCX)
Table S4 (DOCX)
Table S5 (DOCX)